



Publication Year	2019
Acceptance in OA@INAF	2020-12-18T15:19:43Z
Title	Variable Stars in Terzan 5: Additional Evidence of Multi-age and Multi-iron Stellar Populations
Authors	ORIGLIA, Livia; Mucciarelli, A.; FIORENTINO, Giuliana; Ferraro, F. R.; Dalessandro, Emanuele; et al.
DOI	10.3847/1538-4357/aaf730
Handle	http://hdl.handle.net/20.500.12386/29016
Journal	THE ASTROPHYSICAL JOURNAL
Number	871



Variable Stars in Terzan 5: Additional Evidence of Multi-age and Multi-iron Stellar Populations*

L. Origlia¹ , A. Mucciarelli^{1,2} , G. Fiorentino¹ , F. R. Ferraro^{1,2} , E. Dalessandro¹ , B. Lanzoni^{1,2} , R. M. Rich³ ,
D. Massari⁴ , R. Contreras Ramos^{5,6}, and N. Matsunaga⁷

¹ INAF-Osservatorio di Astrofisica e Scienza dello Spazio, Via Gobetti 93/3, I-40129 Bologna, Italy; livia.origlia@inaf.it

² Dipartimento di Fisica e Astronomia, Università degli Studi di Bologna, Via Gobetti 93/2, I-40129 Bologna, Italy

³ Department of Physics and Astronomy, University of California at Los Angeles, 430 Portola Plaza Box 951547, Los Angeles, CA 90095-1547, USA

⁴ Kapteyn Astronomical Institute, University of Groningen, Groningen, Netherlands

⁵ Millennium Institute of Astrophysics, Santiago, Chile

⁶ Instituto de Astrofísica, Pontificia Universidad Católica de Chile, Av. Vicuña Mackenna 4860, 782-0436 Macul, Santiago, Chile

⁷ Department of Astronomy, The University of Tokyo, 7-3-1 Hongo, Bunkyo-ku, Tokyo 113-0033, Japan

Received 2018 October 26; revised 2018 December 7; accepted 2018 December 7; published 2019 January 25

Abstract

Terzan 5 is a complex stellar system in the Galactic bulge, harboring stellar populations (SPs) with very different iron content ($\Delta[\text{Fe}/\text{H}] \sim 1$ dex) and with ages differing by several gigayears. Here we present an investigation of its variable stars. We report on the discovery and characterization of three RR Lyrae stars. For these newly discovered RR Lyrae and for six Miras of known periods we provide radial velocity (RV) and chemical abundances from spectra acquired with X-SHOOTER at the Very Large Telescope. We find that the three RR Lyrae and the three short-period Miras ($P < 300$ days) have RV consistent with being Terzan 5 members. They have subsolar iron abundances and enhanced $[\alpha/\text{Fe}]$, well matching the age and abundance patterns of the 12 Gyr metal-poor SPs of Terzan 5. Only one, out of the three long-period ($P > 300$ days) Miras analyzed in this study, has an RV consistent with being a Terzan 5 member. Its super-solar iron abundance and solar-scaled $[\alpha/\text{Fe}]$ nicely match the chemical properties of the metal-rich SP of Terzan 5 and its derived mass nicely agrees with being several gigayears younger than the short-period Miras. This young variable is an additional proof of the surprisingly young subpopulation discovered in Terzan 5.

Key words: Galaxy: abundances – Galaxy: bulge – infrared: stars – stars: abundances – stars: variables: general – techniques: spectroscopic

1. Introduction

Terzan 5 (hereafter Ter5) is a stellar system commonly cataloged as a globular cluster located in the bulge of the Milky Way (MW). It is affected by large (Ortolani et al. 1996; Barbuy et al. 1998; Valenti et al. 2007) and differential (Massari et al. 2012) reddening, with an average color excess $E(B - V) = 2.38$. This stellar system also harbors an exceptionally large population of millisecond pulsars (MSPs; Ransom et al. 2005; Cadelano et al. 2018). See also the updated list at <http://www.naic.edu/~pfreire/GCpsr.html> and a proto-MSP (Ferraro et al. 2015).

Adaptive optics imaging with the Very Large Telescope (VLT) and near-IR spectroscopy with Keck revealed the presence of two distinct red clumps in the color–magnitude diagram, that cannot be explained by differential reddening or distance effects, while they show very different iron abundances ($[\text{Fe}/\text{H}] = -0.2$ and $+0.3$ dex, respectively, Ferraro et al. 2009). Subsequent spectroscopic studies (Origlia et al. 2011, 2013; Massari et al. 2014a, 2014b) fully confirmed this finding and revealed an additional, minor (a few percent) stellar population (SP) of metal-poor stars at $[\text{Fe}/\text{H}] \sim -0.8$ dex, bringing the overall metallicity range covered by the SPs of Ter5 to ~ 1 dex. Note that such a large iron spread has never been observed in any Galactic globular cluster, with the only

exception being ω Centauri in the halo, which is now believed to be the remnant of a dwarf galaxy accreted by the MW (see, e.g., Bekki & Freeman 2003; Bekki & Norris 2006). The subsolar SPs of Ter5, with peaks at $[\text{Fe}/\text{H}] \sim -0.2$ and -0.8 dex, are α -enhanced and they likely formed early and quickly from a gas mainly polluted by SNe II. The super-solar component at $[\text{Fe}/\text{H}] \sim +0.3$ dex is more centrally concentrated than the others (Ferraro et al. 2009; Lanzoni et al. 2010), and it has approximately solar $[\alpha/\text{Fe}]$ ratio, requiring a progenitor gas polluted by both SNe II and SNe Ia on a longer timescale. Recently, by means of *Hubble Space Telescope* (HST) and ground-based adaptive optics deep imaging, we detected two distinct main-sequence turnoff points in Ter5, providing the age of the two main SPs (Ferraro et al. 2016): 12 Gyr for the (dominant) subsolar component and 4.5 Gyr for the one at super-solar metallicity.

An intriguing scenario is emerging from these observational facts. (i) Ter5 is not a genuine globular cluster or the result of the merging of two globular clusters. (ii) It has experienced a complex star formation (SF) and chemical enrichment history, possibly characterized by short SF episodes (thus accounting for the small metallicity spread measured within each subpopulation). (iii) Ter5 was originally much more massive ($>10^7 M_\odot$) than it is today ($2 \times 10^6 M_\odot$, Lanzoni et al. 2010), and was thus able to retain the SN ejecta. An initial larger mass can also explain its huge population of MSPs. (iv) Lastly, Ter5 seems to have formed and evolved in deep connection with the bulge (Massari et al. 2015).

Indeed, there is a striking chemical similarity between the Ter5 and the bulge SPs, which show a metallicity distribution

* Based on observations collected at the Very Large Telescope of the European Southern Observatory under program 097.D-0337. Also based on observations (GO 10845) with the NASA/ESA *Hubble Space Telescope*, obtained at the Space Telescope Science Institute, which is operated by AURA, Inc., under NASA contract NAS 5-26555.

with two major peaks at subsolar and super-solar $[\text{Fe}/\text{H}]$ and a tail/minor peak toward lower metallicities (see, e.g., Zoccali et al. 2008; Hill et al. 2011; Johnson et al. 2011; Rich et al. 2012; Bensby et al. 2013; Ness et al. 2013a, 2013b, and also Johnson et al. 2014; Rojas-Arriagada et al. 2014; Gonzalez et al. 2015; Ryde et al. 2016; Jönsson et al. 2017; Schultheis et al. 2017). These bulge SPs also show $[\alpha/\text{Fe}]$ enhancement up to about solar metallicity, and then a progressive decline toward solar $[\alpha/\text{Fe}]$ at super-solar $[\text{Fe}/\text{H}]$.

Among the mechanisms that could have contributed to form the Galactic bulge, early (gas and stars) merging, friction of massive clumps, proto-disk evaporation etc. have been proposed over the past several years (see, e.g., Immeli et al. 2004; Carollo et al. 2007; Elmegreen et al. 2008). More recently, it has been suggested that the giant clumps observed in high redshift galaxies (see, e.g., Genzel et al. 2011; Tacchella et al. 2015) could have originated by the clustering of smaller, seed clumps with typical masses of 10^7 – $10^8 M_\odot$ (see e.g., Behrendi et al. 2016), in a bottom-up scenario. In this framework (see, e.g., Ferraro et al. 2016), the proto-Ter5 could have been one of those seed clumps that did not grow and merge into the Galactic bulge, but for some unknown reason evolved in isolation and self-enriched. Very recently, McKenzie & Bekki (2018) suggested that the super-solar component of Ter5 could have originated from the gas of a giant molecular cloud colliding with the proto-Ter5 some gigayears ago.

An important and still unexplored piece of the Ter5 puzzle is its population of variable stars, which represent independent and powerful tracers of SP properties. Indeed, it is well known that, while RR Lyrae trace old (>10 Gyr) SPs, Mira stars with different pulsation periods and metallicity can trace SPs of different ages. Short-period Miras ($P < 300$ days) usually trace old SPs, while long-period ($P > 300$ days) ones are normally younger.

2. Searching for Variables Stars in Ter5

A systematic search for RR Lyrae in Ter5 is still missing. Edmonds et al. (2001) discovered one such candidate star by using *HST*-NICMOS. Recently, we used a sequence of 24 images acquired with the *HST* Wide Field Planetary Camera 2 (WFPC2), obtained through proposal GO-10845 (PI: Ferraro), to identify other candidates. Each image has an exposure time $t_{\text{exp}} = 500$ s. Twelve images have been obtained in the F606W and 12 in the F814W passbands.

In this data set the planetary camera (with the highest spatial resolution of $\sim 0''.046 \text{ px}^{-1}$) is roughly centered on the cluster core. The photometric reduction was performed independently for each image and chip by using *DAOPHOT* (Stetson 1987) and following the approach adopted to study other dense stellar fields (e.g., Dalessandro et al. 2018). Briefly, dozens of bright and isolated stars have been selected in each image to model the point-spread function. A first star list was obtained for each image by independently fitting all the star-like sources at 3σ from the local background. A master-list including all stars detected in at least 13 (i.e., $n/2+1$) images was created and a fit was then forced at the corresponding positions in each frame by using *ALLFRAME* (Stetson 1994). For each image, instrumental magnitudes were corrected for charge transfer efficiency by using the prescriptions described in Dolphin (2000). Different magnitude estimates were homogenized by using *DAOMATCH* and *DAOMASTER* and were then reported to the

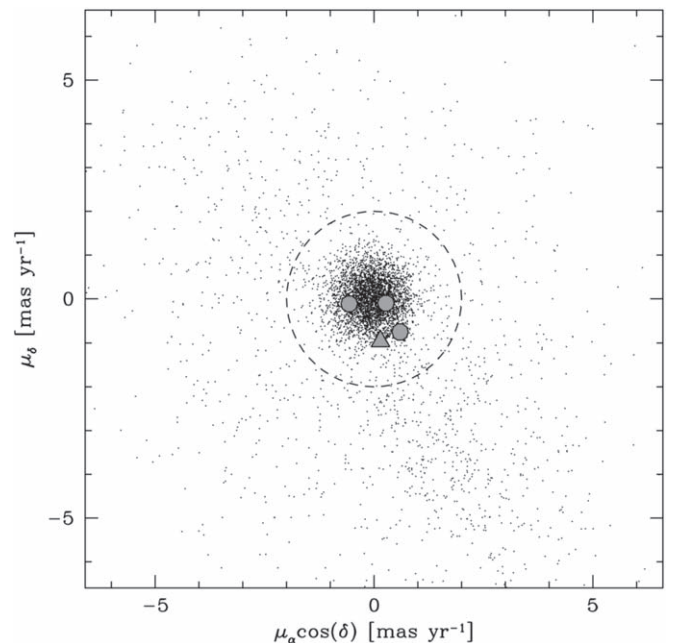


Figure 1. Vector point diagram (VPD) of the *HST* proper motions measured by Massari et al. (2015) for stars with $V < 24$ toward Ter5. The three gray circles are the newly discovered RR Lyrae presented in this work (RR1, RR2, and RR3), while the gray triangle is RR4 (Edmonds et al. 2001). The dashed circle delimits the area in the VPD where likely Ter5 member stars are distributed. Clearly, all RR Lyrae have proper motions fully consistent with the mean motion of Ter5.

VEGAMAG photometric system following Holtzman et al. (1995) and related zero-points. Instrumental coordinates were roto-translated to the absolute coordinate system by using the stars in common with the *HST* catalog used in Ferraro et al. (2009) as a secondary astrometric standard and the cross-correlation software CataXcorr.

By taking advantage of the relatively large number of images in this data set and the photometric quality of *HST*, we performed a detailed variability analysis of stars with magnitudes in the range of $16.5 < m_{\text{F814W}} < 18.5$ (corresponding to the red clump magnitude level) looking for candidate RR Lyrae stars. The analysis of variable stars was carried out in the F606W and F814W bands, separately. As a first diagnostic to identify variables, we used the *variability indicator* provided by *DAOPHOT*. We selected only stars showing variability values significantly larger than those of the bulk of stars with similar magnitudes in both bands. Then we visually checked their preliminary light curves and considered only stars showing coherent evidence of variability in F606W and F814W. We identified in this way four candidate RR Lyrae. It turns out that one of them (RR4) corresponds to the candidate RR Lyrae star V1 found by Edmonds et al. (2001) using near-IR *HST* imagery. The other three are newly discovered candidate variables.

All four variables are located in the central $80''$ (where the contamination by bulge field giants is negligible, of the order of 2%; Massari et al. 2014a, 2014b). For these stars there are *HST* proper motion estimates by Massari et al. (2015), and Figure 1 shows the vector point diagram with the location of Ter5 stars and the four known RR Lyrae. The variables are well clumped within the bulk of the Ter5 distribution, thus providing robust

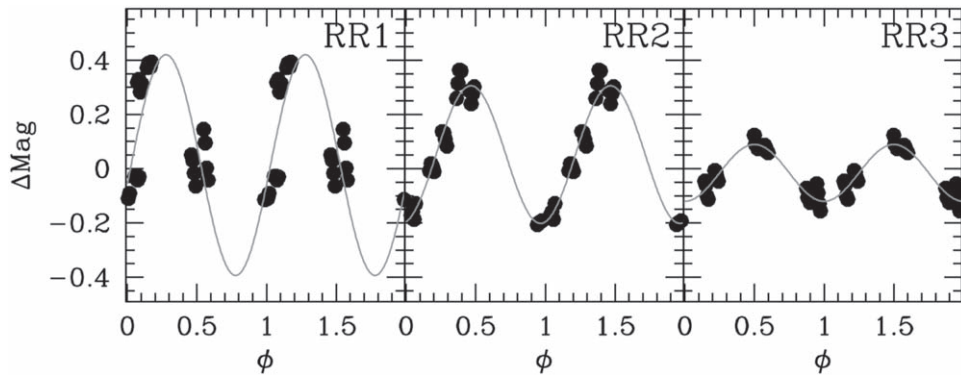


Figure 2. Light curves from *HST* photometry of the three, newly discovered RR Lyrae in Ter5.

evidence for their membership. Because of the reddening, these variables are too faint to be measured by *Gaia*.

We analyzed the light curves of the three new candidate RR Lyrae by using the Graphical Analyzer of Time Series (*GRATIS2*).⁸ It uses both the Lomb periodogram (Lomb 1976) and the best fit of the data with a truncated Fourier series (Barning 1963). The final periods adopted to fold the light curves are those that minimize the rms scatter of the truncated Fourier series that best fit the data.

To use the largest possible sample of data points, for each variable we have scaled the F814W magnitudes to the F606W ones, by using the amplitude ratio $A_{F606W}/A_{F814W} = 1.49$ derived by Fiorentino et al. (2012). The Fourier analysis was then applied to the combined F606W and F814W light curves, shown in Figure 2. For all the candidate RR Lyrae we obtained periods in the 0.6–0.9 day range (see Table 1), typical of fundamental pulsators of AB type.

However, we note that, given the incomplete sampling of the currently available light curves, particularly in the case of RR1, the inferred pulsation periods and especially amplitudes should be considered as indicative. More precise estimates will follow when better sampled light curves become available.

An extensive search for Miras in Ter5 was done by N. Matzunaga for his PhD thesis by using the SIRIUS near-IR camera attached to the 1.4 m Infrared Survey Facility telescope over the period from 2002 to 2005. Among the detected Mira candidates, six are possibly Ter5 members according to their *K*-band magnitudes and period–luminosity (P–L) relation (see Sloan et al. 2010 for a discussion of five such candidates). We note that these six Miras (M1 to M6) are known as V2, V6, V8, V5, V7, and V12, respectively, in the lists of variable stars in Ter5 by Clement et al. (2001), Sloan et al. (2010). Three Miras have periods $P < 300$ days, while the other three stars have periods $P > 300$ days (see Table 1). Moreover, we note that four (M1 to M4) out of these six Miras are located in the inner $100''$, where field contamination by giant stars is negligible, and the other two targets are at distances of about $200''$ from the Ter5 center, where contamination is still reasonably low (about 30%, Massari et al. 2014a, 2014b).

These variables lack proper motions from Massari et al. (2015), because they were saturated in that survey, while they are sufficiently bright for *Gaia*. First proper motion estimates from DR2 (*Gaia* Collaboration et al. 2018) indicate

membership for M1, M2, and M3 and nonmembership for M5 and M6, while no measurements are available for M4.

By combining observed and theoretical pulsation properties of Miras with evolutionary models, Feast (1996) derived the following relation (his Equation (15); see also Wood & Bessell 1983): $\log M/M_{\odot} = 0.470 \log P + 0.356 [\text{Fe}/\text{H}] - 1.340$, that, for a given metallicity, predicts larger masses (i.e., younger ages) for longer pulsation periods. Interestingly, the mass difference between Miras with different pulsation periods becomes even larger if the longer period variables are also more metal-rich. Thus, accurate determination of the metal content of the Mira variables is key to constrain their mass (hence their age) and the properties of their parent SP (e.g., Catchpole et al. 2016).

3. Spectroscopic Observations and Data Analysis

We used X-SHOOTER (Vernet et al. 2011) at the VLT under program 097.D-0337 (PI: L. Origlia), to observe the three most isolated RR Lyrae (namely, RR1, RR2, and RR3)⁹ and the six detected Miras (see Table 1). We selected the VIS and near-IR ARMs to simultaneously acquire spectra in the calcium triplet region with the $0''7$ slit at $R \simeq 11,000$, and in the JHK bands with the $0''6$ slit at $R \simeq 8000$. This allowed us to measure several atomic lines and, in the cool Miras, also molecular CO and OH lines, from which we derived radial velocities (RVs) and chemical abundances. Examples of the observed spectra are shown in Figure 3.

The acquisition of X-SHOOTER spectra has been performed by nodding on slit, with a typical throw of a few arcseconds, for an optimal subtraction of the background and the detector noise. The reduction of the X-SHOOTER spectra has been performed by using the ESO X-SHOOTER pipeline version 3.1.0 to obtain 2D rectified and wavelength calibrated spectra. Order and 1D spectrum extraction has been performed manually. Total on-source exposure times were 11 minutes on Mira variables and 40 minutes on RR Lyrae. Overall signal-to-noise ratios of 30–50 per resolution element have been measured on the final spectra.

For spectral analysis we have used the MARCS model atmospheres (Gustafsson et al. 2008) and the code described in detail in Origlia et al. (2002) and Origlia & Rich (2004), already used to compute synthetic spectra for normal giant stars in Ter5 (Origlia et al. 2011, 2013). The code uses the LTE approximation and it includes thousands of near-IR

⁸ *GRATIS2* is a private software developed at the Bologna Observatory by P. Montegriffo.

⁹ RR4, instead, has several neighbors that complicate its observation with medium-high resolution, seeing-limited spectrographs.

Table 1
Coordinates, Stellar Parameters, and Chemical Abundances for the Observed Variable Stars in Ter5

Header	RR1	RR2	RR3	M1	M2	M3	M4	M5	M6
R.A. (h m s)	17 48 02.8	17 48 08.2	17 48 04.3	17 47 59.5	17 48 09.3	17 48 07.2	17 48 03.4	17 47 54.3	17 47 53.2
Decl. ($^{\circ}$ ' ")	-24 47 47.5	-24 45 42.1	-24 47 37.7	-24 47 17.6	-24 47 06.3	-24 46 26.6	-24 46 42.0	-24 49 54.6	-24 44 34.0
P (days)	0.72	0.64	0.89	217	269	261	464	377	455
Phase ^a	0.70	0.49	0.63	0.61	0.38	0.51	0.73	0.42	0.35
T_{eff}	6250	6000	6000	3100	3400	3000	3000	3100	3200
RV ^b	-77	-98	-92	-89	-95	-75	-119	+162	+48
[Fe/H]	-0.72 \pm 0.03	-0.71 \pm 0.03	-0.67 \pm 0.01	-0.27 \pm 0.01	-0.33 \pm 0.05	-0.26 \pm 0.07	+0.32 \pm 0.01	+0.27 \pm 0.01	+0.31 \pm 0.05
[Ca/Fe]	+0.27 \pm 0.15	+0.37 \pm 0.04	+0.35 \pm 0.03	+0.31 \pm 0.15	+0.30 \pm 0.16	+0.32 \pm 0.17	+0.06 \pm 0.15	-0.04 \pm 0.06	-0.02 \pm 0.16
[Si/Fe]	+0.39 \pm 0.16	+0.36 \pm 0.15	+0.37 \pm 0.03	+0.38 \pm 0.15	+0.40 \pm 0.16	+0.30 \pm 0.17	+0.02 \pm 0.03	-0.03 \pm 0.15	-0.05 \pm 0.06
[Mg/Fe]	+0.35 \pm 0.15	+0.31 \pm 0.15	+0.36 \pm 0.03	+0.45 \pm 0.15	+0.36 \pm 0.09	+0.33 \pm 0.10	-0.00 \pm 0.15	-0.01 \pm 0.15	-0.01 \pm 0.16
[Ti/Fe]	+0.22 \pm 0.15	+0.31 \pm 0.15	+0.29 \pm 0.15	+0.35 \pm 0.02	+0.25 \pm 0.05	+0.33 \pm 0.09	-0.06 \pm 0.03	-0.06 \pm 0.07	-0.02 \pm 0.16
[Al/Fe]	+0.25 \pm 0.15	+0.28 \pm 0.15	+0.36 \pm 0.03	+0.36 \pm 0.03	+0.41 \pm 0.06	+0.41 \pm 0.07	-0.07 \pm 0.09	+0.13 \pm 0.02	-0.05 \pm 0.07
[Na/Fe]	-0.07 \pm 0.15	+0.04 \pm 0.15	-0.07 \pm 0.15	-0.01 \pm 0.15	+0.01 \pm 0.16	+0.08 \pm 0.17	+0.00 \pm 0.03	+0.07 \pm 0.15	-0.01 \pm 0.16
[Mn/Fe]	+0.04 \pm 0.15	+0.05 \pm 0.16	-0.03 \pm 0.17	-0.07 \pm 0.15	-0.01 \pm 0.15	-0.02 \pm 0.16
[K/Fe]	-0.06 \pm 0.15	+0.02 \pm 0.19	-0.06 \pm 0.17	-0.02 \pm 0.15	-0.03 \pm 0.15	-0.07 \pm 0.16
[O/Fe]	+0.32 \pm 0.04	+0.41 \pm 0.12	+0.44 \pm 0.18	-0.08 \pm 0.12	-0.01 \pm 0.02	+0.03 \pm 0.10

Notes.

^a Approximative phase at the epoch of the spectroscopic observation with X-SHOOTER.

^b Heliocentric radial velocity in kilometers per second, with typical uncertainties of ± 2 km s⁻¹.

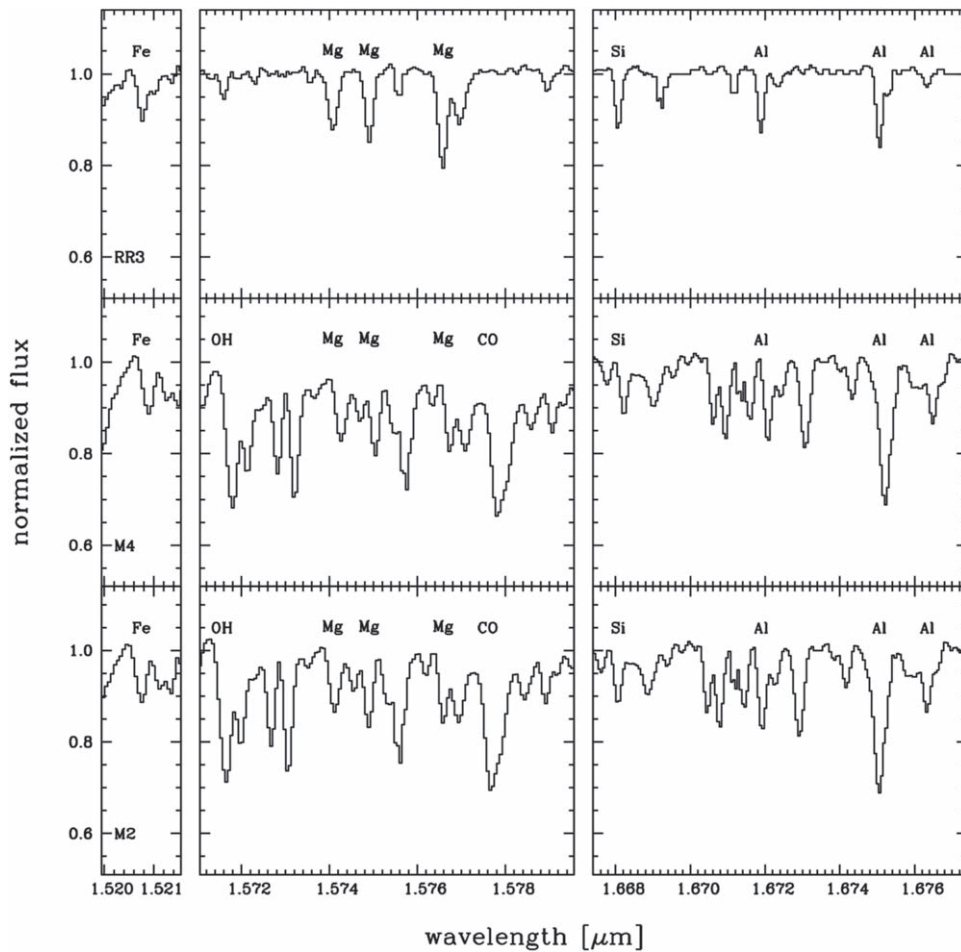


Figure 3. Portions of the observed spectra of the M2, M4, and RR3 variable stars of Ter5 around some features of interest.

atomic transitions from the Kurucz database,¹⁰ Bièmont & Grevesse (1973), and Meléndez & Barbuy (1999), while molecular data are taken from our (Origlia et al. 1993, 1997, and subsequent updates) and B. Plez’s (2018, private communications) compilations. We use the Grevesse & Sauval (1998) abundances for the solar reference. A list of suitable lines for each measurable chemical element, free from significant blending and/or contamination by telluric absorption and without strong wings, has been identified. Chemical abundances have been derived by minimizing the scatter between observed and synthetic spectra with suitable photospheric parameters and also using as a figure of merit equivalent width measurements of selected lines. The typical random error of the measured line equivalent widths is 20–30 mÅ, mostly arising from a $\pm 1\%$ – 2% uncertainty in the placement of the pseudo-continuum, as estimated by overlapping the synthetic and the observed spectra. This error corresponds to abundance variations of about 0.1 dex, comparable with the typical 1σ scatter (≤ 0.15 dex) in the derived abundances from different lines. The errors quoted in Table 1 for the final abundances were obtained by dividing the 1σ scatter by the square root of the number of used lines, typically a few per species. When only one line was available, we assumed a 0.15 dex error.

4. Results

Neutral atomic lines in the *H*-band have been used to derive abundances of Fe, Ca, Si, Mg, Ti, and Al. Additional atomic lines of Mg, Al, Na, K, and Mn in the *J*-band and of Ti, Al, and Na in the *K*-band have also been used to derive abundances for the corresponding metals. These lines have also been used to derive heliocentric RVs. OH lines in the spectra of the cool Miras have been used to derive abundances of O in those variables. Detailed information on the best-fit estimates of the stellar parameters, final RVs, and chemical abundances for the observed variables are given in the next two subsections.

4.1. RR Lyrae Variables

The three observed RR Lyrae stars have quite long periods. Although, these are typical of metal-poor systems (Fiorentino et al. 2015), they may also be detected in systems with a red horizontal branch morphology, as is observed in the metal-rich SPs of the bulge and its globular clusters (e.g., Kunder et al. 2016, 2018, and references therein).

Given that the stellar parameters of the RR Lyrae stars vary with the pulsation period, we have computed theoretical models (see Marconi et al. 2013 for details) for the inferred long periods and for metallicities between solar and one-tenth solar, and predict corresponding RV, effective temperature (T_{eff}), and gravity ($\log g$) variability curves. We have found maximum amplitudes of about ± 20 km s⁻¹ in RV with respect

¹⁰ <http://www.cfa.harvard.edu/amp/ampdata/kurucz23/sekur.html>

to the average one, 600 K in T_{eff} , and 0.5 dex in $\log g$. These predictions, coupled with the spectroscopic observation epoch, allow us to provide first guess RV, T_{eff} and $\log g$. We thus computed a grid of synthetic spectra with varying abundances and stellar parameters according to the variability curves. Best-fit estimates from spectral synthesis turned out to be in excellent agreement with those predicted by the variability curves at the epoch of the spectroscopic observation and fully consistent with those expected for stars in the instability strip.

An average microturbulence velocity of 2 km s^{-1} and $\log g$ of 3.0 dex have been assumed for all the stars, while the adopted temperatures ($\geq 6000 \text{ K}$) are reported in Table 1. Systematic uncertainties of $\pm 200 \text{ K}$ in T_{eff} , ± 0.5 in $\log g$ and $\pm 0.5 \text{ km s}^{-1}$ in microturbulence velocity have been considered, and their impact on individual abundances turns out to be ≤ 0.1 dex, while the abundance ratios are practically unaffected.

The systemic velocity of Ter5 is $\approx -83 \text{ km s}^{-1}$ and its velocity dispersion in the central region is $\approx 15 \text{ km s}^{-1}$ and its (Massari et al. 2014b). Hence, according to the measured RVs (see Table 1), all the three observed RR Lyrae are fully consistent with being Ter5 members.

The derived chemical abundances and abundance ratios of Fe, Ca, Si, Mg, Ti, Al, and Na are listed in Table 1 and plotted in Figure 4. An iron abundance $[\text{Fe}/\text{H}] \sim -0.7$ dex, enhanced $[\alpha/\text{Fe}]$ and $[\text{Al}/\text{Fe}]$, and solar-scaled $[\text{Na}/\text{Fe}]$ have been homogeneously inferred for the three RR Lyrae.

This metallicity, together with the best-fit periods and the average V magnitudes, can also be used to constrain the distance of Ter5, by means of the period–luminosity relation by Catelan et al. (2004). V magnitudes in the Johnson–Cousin system have been obtained from the mean magnitudes in the *HST* filters and photometric transformations computed by using the stars in common between the WFPC2 data set used in the present work and the ACS catalog published by Ferraro et al. (2009). We found V magnitudes of 21.77, 22.59, and 21.83 for RR1, RR2, and RR3, respectively. The proper extinction value was then associated with each candidate RR Lyrae star by using the differential reddening map derived by Massari et al. (2012). We obtain a distance $d = 6.6_{-1.6}^{+2.0} \text{ kpc}$, $5.9_{-1.5}^{+1.9} \text{ kpc}$, and $5.9_{-1.5}^{+2.0} \text{ kpc}$ for RR1, RR2, and RR3 respectively. The errors are obtained by assuming a 10% uncertainty on the adopted $E(B - V)$ values. The derived values match the distance of $5.9 \pm 0.5 \text{ kpc}$ obtained by Valenti et al. (2007) from IR photometry of the Red Giant Branch (RGB) of Ter5.

Interestingly, the period–metallicity distribution of the Ter5 RR Lyrae stars resembles that of the RR Lyrae in the bulge globular clusters NGC 6388 and NGC 6441 (see, e.g., Pritzl et al. 2000, and references therein). However, the uncertainty in the amplitude estimates from the current light curves prevent us from using their period–amplitude distribution as a diagnostic tool for checking their possible association with a population of super-luminous, He-rich stars, as suggested for NGC 6388 and NGC 6441 (Rich et al. 1997; Pritzl et al. 2002; Busso et al. 2007; Brown et al. 2016; Tailo et al. 2017).

4.2. Mira Variables

Very few spectroscopic studies on Mira variables exist in general, and most of them have been focused on the complex kinematics of their atmospheres (e.g., Hinkle 1978; Hinkle et al. 1982; Lebzelter et al. 2005; Wittkowski et al. 2011) and occasionally on the determination of C/O abundance ratios (e.g., Lebzelter et al. 2014; Hinkle et al. 2016) from molecular

CO and OH lines in near-IR spectra. However, very recently and for the first time, some iron, α -element, and sodium abundances of a Mira star in the globular cluster NGC 5927 have been measured by D’Orazi et al. (2018), using J -band spectroscopy.

Mira variables have complex atmospheres, characterized by substructures with different [low] temperatures, gravities, and velocity fields, that also change with the pulsational phase. A cool photosphere with temperatures as low as $\approx 3000 \text{ K}$ is believed to be the source of the atomic lines, as well as of most of the molecular CO and OH features. However, especially near the maximum, a $\approx 1000 \text{ K}$ gaseous component likely in the inner portion of a circumstellar shell, can contribute to low-excitation molecular absorption lines. Moreover, velocity gradients, departure from LTE in the outer layers, and/or P Cygni type emission arising in a circumstellar shell might weaken some absorption lines. Although hydrostatic model atmospheres cannot satisfactorily reproduce all the observed features, especially near the maximum, they can still be used to perform some chemical abundance analysis from high excitation atomic and molecular lines that originate in the innermost region of Mira’s photosphere.

The six candidate Miras toward Ter5 have been observed at a random phase far from the maximum (see Table 1). Effective temperatures have been spectroscopically determined from X-SHOOTER spectra, by computing the CO indices in correspondence with the first-overtone (2–0) and (3–1) band-heads in the K -band and using the calibrations reported in Schultheis et al. (2016). We find values in the 3000–3400 K range (see Table 1), consistent with an observation epoch far from the light-curve maximum. A microturbulence velocity of 2 km s^{-1} and a surface gravity $\log g$ of 0.5 dex have been adopted, consistent with the typical values measured in Ter5 nonvariable cool giants near the RGB tip (Origlia et al. 2011, 2013). Systematic uncertainties of $\pm 200 \text{ K}$ in T_{eff} , ± 0.5 in $\log g$ and $\pm 0.5 \text{ km s}^{-1}$ in microturbulence velocity imply abundance variations between 0.1 and 0.2 dex.

Second overtone molecular band-heads of ^{12}CO have been routinely used to derive carbon abundances in normal RGB stars. However, in pulsating Miras, these band-heads can be affected by kinematics, thus making it difficult to disentangle abundance from velocity gradient effects. Hence, we did not attempt to obtain any carbon abundance estimate from the spectral synthesis.

According to the measured RVs (see Table 1), only the innermost Miras (M1 to M4) are consistent with being Ter5 members, which is also in agreement with the proper motions measured by *Gaia*. M4 has been observed after its minimum of luminosity, hence its RV is expected to be negative with respect to the mean. The measured value of -119 km s^{-1} , although significantly more negative than the other Miras and the systemic velocity, is still consistent with a Ter5 membership at the ≈ 1.5 – 2.0σ level. Interestingly, Matsunaga et al. (2005) detected SiO maser emission of M4 at $V(\text{LSR}) = -106 \text{ km s}^{-1}$, which corresponds to -96 km s^{-1} , giving an additional, strong support for the membership of this star.

The derived chemical abundances and abundance ratios of Fe, Ca, Si, Mg, Ti, Al, Na, Mn, K, and O are listed in Table 1 and plotted in Figure 4. An iron abundance $[\text{Fe}/\text{H}] \sim -0.3$ dex, enhanced $[\alpha/\text{Fe}]$ and $[\text{Al}/\text{Fe}]$, and about solar-scaled $[\text{Mn}/\text{Fe}]$, $[\text{Na}/\text{Fe}]$, and $\text{K}[\text{Fe}]$ have been inferred for the three Miras M1, M2, and M3 with $P < 300$ days, while M4

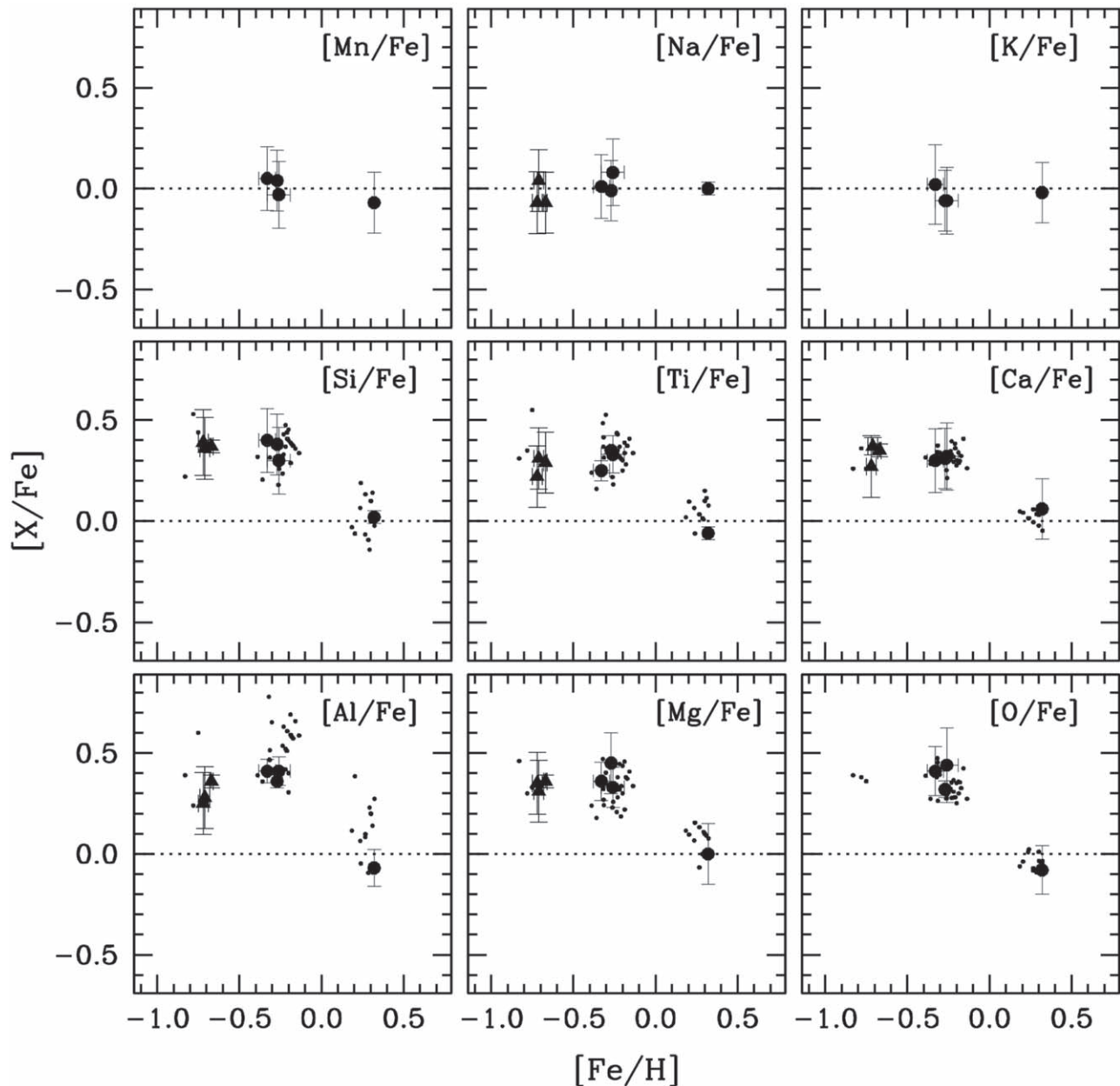


Figure 4. Abundance ratios $[X/Fe]$ as a function of $[Fe/H]$ for the member RR Lyrae (filled triangles), Mira variables (large circles), and normal RGB stars (small dots, from Origlia et al. 2011, 2013) of Ter5.

and the other two Miras with longer periods ($P > 300$ days) have super-solar iron ($[Fe/H] \sim +0.3$ dex) and about solar-scaled $[\alpha/Fe]$, $[Al/Fe]$, $[Na/Fe]$, $[Mn/Fe]$, and $[K/Fe]$.

5. Discussion and Conclusion

The seven variables (three RR Lyrae and four Miras) that have been found to have RVs consistent with being members of Ter5 have very different metallicities and $[\alpha/Fe]$ abundance ratios. The agreement with the earlier nonvariable star studies of M giants in Ter5 (Origlia et al. 2011, 2013) is striking. The three RR Lyrae show $[Fe/H] \sim -0.7$ dex and enhanced $[\alpha/Fe] \sim +0.3$ dex, nicely matching the values obtained for the most metal-poor population detected in Ter5 (Origlia et al. 2013, see also Figure 4). The three Miras with $P < 300$ days (namely, M1, M2, and M3) appear to be clumped at $[Fe/H] \sim -0.3$ dex and $[\alpha/Fe] \sim +0.3$ dex, again nicely matching the values measured

in the dominant subsolar population of Ter5. The exceptionally long-period Mira M4 at $[Fe/H] = +0.32$ and solar-scaled $[\alpha/Fe]$ is fully consistent with the super-solar component that Ferraro et al. (2016) found to be 7 Gyr younger than the metal-poor SPs of Ter5. Consistently, the mass of the M4 Mira is expected to be significantly larger than the mass of the other Ter5 Miras (M1, M2, and M3) at lower metallicity and with significantly shorter periods. Indeed, we note that an increase in the He content and/or a super-solar metallicity alone are not sufficient to explain the long period of M4. By using Equation (15) in Feast (1996) we obtain a current mass of $\sim 0.5 M_{\odot}$ for M1, M2, and M3 and $\sim 1 M_{\odot}$ for M4, that is a difference in mass of $\Delta M \sim 0.5 M_{\odot}$. This value is in nice agreement with the mass difference $\Delta M_{TO} \sim 0.4 M_{\odot}$ that Ferraro et al. (2016) measured at the main-sequence turnoff for the two subpopulations of Ter5 (i.e., $M_{TO} = 0.92$ for the 12 Gyr old and subsolar metallicity









component, and $1.32 M_{\odot}$ for the 4.5 Gyr old and super-solar metallicity one).

Interestingly, the other two long-period Miras, namely M5 and M6, which are likely bulge field stars, have abundances and abundance patterns similar to those of M4, providing additional evidence of the connection between Ter5 and the bulge, and of young ages for some stars in both systems.

Finally, our finding that both the RR Lyrae and Mira variables in Ter5 have metallicities and ages consistent with those of nonvariable stars is a confirmation of the scenario proposed in Ferraro et al. (2016, and references therein), where Ter5 experienced a complex evolutionary history and is currently comprised of subpopulations with multiple and discrete ages and metallicities.

E.D. acknowledges support from The Leverhulme Trust Visiting Professorship Programme VP2-2017-030. R.M.R. acknowledges support from grants AST-1413755, 1518271 from the National Science Foundation. D.M. acknowledges financial support from a Vici grant from NWO. This research is part of the Cosmic-Lab Project at the Bologna University.

ORCID iDs

L. Origlia  <https://orcid.org/0000-0002-6040-5849>
 A. Mucciarelli  <https://orcid.org/0000-0001-9158-8580>
 G. Fiorentino  <https://orcid.org/0000-0003-0376-6928>
 F. R. Ferraro  <https://orcid.org/0000-0002-2165-8528>
 E. Dalessandro  <https://orcid.org/0000-0003-4237-4601>
 B. Lanzoni  <https://orcid.org/0000-0001-5613-4938>
 R. M. Rich  <https://orcid.org/0000-0003-0427-8387>
 D. Massari  <https://orcid.org/0000-0001-8892-4301>

References

- Barbuy, B., Bica, E., & Ortolani, S. 1998, *A&A*, **333**, 117
 Barning, F. J. M. 1963, *BAN*, **17**, 22
 Behrendi, M., Burkert, A., & Schartmann, M. 2016, *ApJ*, **819**, 2
 Bekki, K., & Freeman, K. C. 2003, *MNRAS*, **346**, L11
 Bekki, K., & Norris, J. E. 2006, *ApJ*, **637**, 109
 Bensby, T., Yee, J.-C., Feltzing, S., et al. 2013, *A&A*, **549**, 147
 Bièmont, E., & Grevesse, N. 1973, *ADNDT*, **12**, 221
 Brown, T. M., Cassisi, S., D'Antona, F., et al. 2016, *ApJ*, **822**, 44
 Busso, G., Cassisi, S., Piotto, G., et al. 2007, *A&A*, **474**, 105
 Cadelano, M., Ransom, S. M., Freire, P. C. C., et al. 2018, *ApJ*, **855**, 125
 Carollo, C. M., Scarlata, C., Stiavelli, M., Wyse, R. F. G., & Mayer, L. 2007, *ApJ*, **658**, 960
 Catchpole, R. M., Whitelock, P. A., Feast, M. W., et al. 2016, *MNRAS*, **455**, 2216
 Catelan, M., Pritzl, B. J., & Smith, H. A. 2004, *ApJS*, **154**, 633
 Clement, C. M., Muzzin, A., Dufton, Q., et al. 2001, *AJ*, **122**, 2587
 Dalessandro, E., Cadelano, M., Vesperini, E., et al. 2018, *ApJ*, **859**, 15
 Dolphin, A. E. 2000, *PASP*, **112**, 1397
 D'Orazi, V., Magurno, D., Bono, G., et al. 2018, *ApJ*, **855**, 9
 Edmonds, P. D., Grindlay, J. E., Cohn, H., & Lugger, P. 2001, *ApJ*, **547**, 829
 Elmegreen, B. G., Bournaud, F., & Elmegreen, D. M. 2008, *ApJ*, **688**, 77
 Feast, M. W. 1996, *MNRAS*, **278**, 11
 Ferraro, F. R., Beccari, G., Dalessandro, E., et al. 2009, *Natur*, **462**, 483
 Ferraro, F. R., Massari, D., Dalessandro, E., et al. 2016, *ApJ*, **828**, 75
 Ferraro, F. R., Pallanca, C., Lanzoni, B., et al. 2015, *ApJL*, **807**, L1
 Fiorentino, G., Bono, G., Monelli, M., et al. 2015, *ApJL*, **798**, L12
 Fiorentino, G., Contreras Ramos, R., Tolstoy, E., Clementini, G., & Saha, A. 2012, *A&A*, **539**, 138
 Gaia Collaboration, Brown, A. G. A., Vallenari, A., et al. 2018, *A&A*, **616**, A1
 Genzel, R., Newman, S., Jones, T., et al. 2011, *ApJ*, **733**, 101
 Gonzalez, O., Zoccali, M., Vasquez, S., et al. 2015, *A&A*, **584**, 46
 Grevesse, N., & Sauval, A. J. 1998, *SSRv*, **85**, 161
 Gustafsson, B., Edvardsson, B., Eriksson, K., et al. 2008, *A&A*, **486**, 951
 Hill, V., Lecureur, A., Gomez, A., et al. 2011, *A&A*, **535**, 80
 Hinkle, K. H. 1978, *ApJ*, **220**, 210
 Hinkle, K. H., Hall, D. B., & Ridgway, S. T. 1982, *ApJ*, **252**, 697
 Hinkle, K. H., Lebzelter, T., & Straniero, O. 2016, *ApJ*, **825**, 38
 Holtzman, J. A., Burrows, C. J., Casertano, S., et al. 1995, *PASP*, **107**, 1065
 Immeli, A., Samland, M., Gerhard, O., & Westera, P. 2004, *A&A*, **413**, 547
 Johnson, C. I., Rich, R. M., Fulbright, J. P., Valenti, E., & McWilliam, A. 2011, *ApJ*, **732**, 108
 Johnson, C. I., Rich, R. M., Kobayashi, C., Kunder, A., & Kock, A. 2014, *AJ*, **148**, 67
 Jönsson, H., Ryde, N., Schultheis, M., & Zoccali, M. 2017, *A&A*, **598**, 101
 Kunder, A., Mills, A., Edgcomb, J., et al. 2018, *AJ*, **155**, 171
 Kunder, A., Rich, R. M., Koch, A., et al. 2016, *ApJ*, **821**, 25
 Lanzoni, B., Ferraro, F. R., Dalessandro, E., et al. 2010, *ApJ*, **717**, 653
 Lebzelter, T., Wood, P. R., Hinkle, K. H., Joyce, R. R., & Fekel, F. C. 2005, *A&A*, **432**, 207
 Lebzelter, T., Wood, P. R., Nowotny, W., et al. 2014, *A&A*, **567**, 143
 Lomb, N. R. 1976, *Ap&SS*, **39**, 447
 Marconi, M., Molinaro, R., Ripepi, V., Musella, I., & Brocato, E. 2013, *MNRAS*, **428**, 2185
 Massari, D., Dalessandro, E., Ferraro, F. R., et al. 2015, *ApJ*, **810**, 69
 Massari, D., Mucciarelli, A., Dalessandro, E., et al. 2012, *ApJ*, **755**, 32
 Massari, D., Mucciarelli, A., Ferraro, F. R., et al. 2014a, *ApJ*, **791**, 101
 Massari, D., Mucciarelli, A., Ferraro, F. R., et al. 2014b, *ApJ*, **795**, 22
 Matsunaga, N., Deguchi, S., Ita, Y., Tanabe, T., & Nakada, Y. 2005, *PASJ*, **57**, L1
 McKenzie, M., & Bekki, K. 2018, *MNRAS*, **479**, 3126
 Meléndez, J., & Barbuy, B. 1999, *ApJS*, **124**, 527
 Ness, M., Freeman, K., Athanassoula, E., et al. 2013a, *MNRAS*, **430**, 836
 Ness, M., Freeman, K., Athanassoula, E., et al. 2013b, *MNRAS*, **432**, 2092
 Origlia, L., Ferraro, F. R., Fusi Pecci, F., & Oliva, E. 1997, *A&A*, **321**, 859
 Origlia, L., Massari, D., Rich, R. M., et al. 2013, *ApJ*, **779**, 5
 Origlia, L., Moorwood, A. F. M., & Oliva, E. 1993, *A&A*, **280**, 536
 Origlia, L., & Rich, R. M. 2004, *AJ*, **127**, 3422
 Origlia, L., Rich, R. M., & Castro, S. 2002, *AJ*, **123**, 1559
 Origlia, L., Rich, R. M., Ferraro, F. R., et al. 2011, *ApJ*, **726**, 20
 Ortolani, S., Barbuy, B., & Bica, E. 1996, *A&A*, **308**, 733
 Pritzl, B., Smith, H. A., Catelan, M., & Sweigart, A. V. 2000, *ApJ*, **530**, 41
 Pritzl, B. J., Smith, H. A., Catelan, M., & Sweigart, A. V. 2002, *AJ*, **124**, 949
 Ransom, S. M., Hessels, J. W. T., Stairs, I. H., et al. 2005, *Sci*, **307**, 892
 Rich, R. M., Origlia, L., & Valenti, E. 2012, *ApJ*, **746**, 59
 Rich, R. M., Sosin, C., Djorgovski, S. G., et al. 1997, *ApJ*, **484**, 25
 Rojas-Arriagada, A., Recio-Blanco, A., Hill, V., et al. 2014, *A&A*, **569**, 103
 Ryde, N., Schultheis, M., Grieco, V., et al. 2016, *ApJ*, **831**, 40
 Schultheis, M., Rojas-Arriagada, A., Garcia-Perez, A. E., et al. 2017, *A&A*, **600**, 14
 Schultheis, M., Ryde, N., & Nandakumari, G. 2016, *A&A*, **590**, 6
 Sloan, G. C., Matsunaga, N., Matsuura, M., et al. 2010, *ApJ*, **719**, 1274
 Stetson, P. B. 1987, *PASP*, **99**, 191
 Stetson, P. B. 1994, *PASP*, **106**, 250
 Tacchella, S., Lang, P., Carollo, C. M., et al. 2015, *ApJ*, **802**, 101
 Tailo, M., D'Antona, F., Milone, A. P., et al. 2017, *MNRAS*, **465**, 1046
 Valenti, E., Ferraro, F. R., & Origlia, L. 2007, *AJ*, **133**, 1287
 Vernet, J., Dekker, H., D'Odorico, S., et al. 2011, *A&A*, **536**, 105
 Wittkowski, M., Boboltz, D. A., Ireland, M., et al. 2011, *A&A*, **532**, 7
 Wood, P. R., & Bessell, M. S. 1983, *ApJ*, **265**, 748
 Zoccali, M., Hill, V., Lecureur, A., et al. 2008, *A&A*, **486**, 177